Biomaterials Science

rsc.li/biomaterials-science

ROYAL SOCIETY
OF **CHEMISTRY**

PAPER
Yan Lee, Sung Bae Park *et al.*
Calcium-binding PLGA microparticles releasing
rhBMP-2 for enhancement of bone healing with
minimal ectopic bone formation in spine fusion

European
Society for
Biomaterials

PAPER

Calcium-binding PLGA microparticles releasing rhBMP-2 for enhancement of bone healing with minimal ectopic bone formation in spine fusion

Minjae Kim,†[a] Jungwoo Kim,†[b] Minji Kang,†[a] So Hee Nam,[c] Chi Heon Kim,[d,e] Yan Lee [ID] *‡[a] and Sung Bae Park*‡[b,d]

We designed a delivery vehicle that can maintain the local concentration of recombinant human bone morphogenetic protein-2 (rhBMP-2) only around the bone surgery site for the enhancement of bone healing without excessive bone formation at non-targeted sites. The microparticles were fabricated by encapsulation of rhBMP-2 into a poly(lactic-*co*-glycolic acid) (PLGA) core and by coating with poly(butyl methacrylate-*co*-methacryloyloxyethyl phosphate) (PBMP), which contains both calcium-binding phosphomonoester groups and PLGA-binding butyl groups. The PBMP-coated PLGA microparticles (PLGA/PBMP) successfully encapsulated rhBMP-2 without compromising its bioactivity and demonstrated encapsulation efficiencies and release kinetics similar to uncoated PLGA microparticles. Notably, the PBMP coating conferred a significantly higher bone-binding affinity compared to PLGA alone. This enhanced binding led to a higher local concentration of rhBMP-2, which in turn significantly upregulated osteogenic markers in preosteoblast MC3T3-E1 cells. We then evaluated the bone growth and ectopic bone formation after treatment with rhBMP-2-encapsulating PLGA/PBMP (BMP-2-PLGA/PBMP) in a rat model of spine fusion surgery using autologous iliac bone. The results revealed that the sustained release of rhBMP-2 from PLGA/PBMP could gradually stimulate bone growth, while free rhBMP-2 boosted bone regeneration only during the first few weeks. More importantly, unlike free rhBMP-2 which showed a high incidence of ectopic bone formation (>60%), BMP-2-PLGA/PBMP showed almost no incidence of ectopic bone formation (≤10%), indicating site-specific delivery. Collectively, our study demonstrates that the PLGA/PBMP microparticle system has great potential for enhancing bone regeneration by enabling localized delivery of rhBMP-2 with minimal side effects.

1. Introduction

Osteoinductive and osteoconductive functions are essential for positive bone formation, remodelling, and bone healing after injury. Osteogenic cells play important roles in the processes;[1] however, decreased numbers and weak potency of osteogenic cells in elderly patients significantly hamper the processes.[2] As a result, the prevalence of delayed bone healing and non-union was reported as up to 61% in elderly patients and the impaired bone formation is common for them even after the bone healing.[3–5] Generally, autobone grafting is considered as the gold standard technique for enhancing osteoinduction for elderly patients.[6] Additionally, bone substitutes are often required for the patients to augment bone formation and to decrease non-union.[6,7]

To enhance osteoinduction during bone healing, various osteoinductive or osteopromotive materials including growth factors, inorganic composites, ceramics, and nanostructured composites have been developed. These materials stimulate the differentiation of mesenchymal stem cells into osteogenic cells and promote bone growth and repair.[1,8] Among them, bone morphogenetic proteins (BMPs), especially BMP-2 and BMP-7, are the most potent osteogenic factors but their clinical use is limited by their short half-life, rapid clearance, and side effects.[9–11] While high-dose treatment of BMPs can overcome their poor pharmacokinetics for effective osteoinduction, this approach may provoke adverse side effects such as excessive bone formation caused by the diffusion of BMPs to non-targeted tissues.[12]

To address these limitations, a variety of biomaterials have been developed to regulate the spatiotemporal release of

[a]Department of Chemistry, Seoul National University, Seoul, Korea.
E-mail: gacn@snu.ac.kr
[b]Department of Neurosurgery, Seoul National University Boramae Medical Center,
Seoul, Korea. E-mail: ddolbae01@snu.ac.kr
[c]College of Pharmacy, Dongduk Women's University, Seoul, Korea
[d]Department of Neurosurgery, Seoul National University College of Medicine, Seoul,
Korea
[e]Clinical Research Institute, Seoul National University Hospital, Seoul, Korea
†Co-first authors: these authors contributed equally to this work.
‡These authors contributed equally to this work.

BMP-2, aiming to minimize side effects and enhance bone regeneration. For instance, injectable hydrogels based on temperature-responsive polymers can conformally fill defect sites while providing sustained release of BMP-2.[13,14] Additionally, 3D-printed scaffolds composed of polycaprolactone (PCL) and β-tricalcium phosphate (β-TCP) have shown the ability to support tissue ingrowth.[15,16]

Another notable approach involves poly(lactide-co-glycolide) (PLGA)-based microparticles and scaffolds. PLGA is one of the most widely used biodegradable polymers approved by the FDA. Due to its endogenous degradation and metabolization into naturally occurring by-products, PLGA exhibits excellent biocompatibility with minimal toxicity. Fine-tuning the ratio of lactic to glycolic acid monomers enables controlled drug release kinetics through hydrolysis of the polyester backbone under physiological conditons.[17–19] Given that bone regeneration typically requires gradual BMP release for at least 4 to 8 weeks for appropriate bone formation, PLGA-based materials have been widely used for bone regeneration applications.[20,21]

Despite these advancements, several challenges remain. One major limitation is the insufficient affinity of delivery vehicles to the target bone defect site, which compromises their retention and anchoring. This weak interfacial interaction often results in premature diffusion of BMP-2 away from the intended site, leading to reduced regenerative efficacy and undesired ectopic bone formation.[10,22] Consequently, researchers have sought to develop sustained-release strategies that enable controlled and localized delivery of BMPs near bone defect sites. Such approaches aim to ensure prolonged exposure, promote effective bone healing and regeneration, and minimize adverse effects associated with BMP leakage.[12]

Our group previously developed a drug delivery system with strong binding affinity to calcium-based surfaces for selective release of drugs around the bone or teeth.[23] PLGA microparti-cles are coated with poly(butyl methacrylate-co-methacryloylox-yethyl phosphate) (PBMP) to introduce strong calcium-binding affinity due to the phosphomonoester side chains. The resulting PBMP-coated PLGA microparticles can slowly release encapsulated small drugs on the surface of hydroxyapatite and exposed bones, successfully inhibiting the bacterial biofilm formation or surgery-induced osteitis in the sinonasal cavity in mice.[23,24] We envisioned that this system could also be applied to the localized delivery of protein-based drugs during the bone surgery.

In this study, we encapsulate recombinant human BMP-2 (rhBMP-2) in the PBMP-coated PLGA microparticles (PLGA/PBMP) and apply the particles to spine fusion surgery using autologous iliac bone (AIB) (Fig. 1), which is a standard technique in the clinic to support bone formation and to decrease non-union for elderly patients.[6] By using the rat AIB model, we analysed the enhancement of local bone formation and the effect of localized delivery of rhBMP-2 encapsulated in PLGA/PBMP on excessive bone formation at non-targeted lesions. These approaches aim to optimize the therapeutic efficacy of BMP-2, promote local bone healing, and facilitate successful bone regeneration with minimal side effects for overcoming the patients' age and medical history, including osteoporosis using an animal model.

2. Materials and methods

2.1 Materials

Poly(D,L-lactide-co-glycolide) (PLGA; average M_w = 54 000–69 000; lactide : glycolide = 50 : 50) was purchased from Evonik (Essen, Germany). 2-Hydroxyethyl methacrylate (HEMA), pyridine, n-butyl methacrylate (BMA), chloroform, 2,2-azobis(2-methylpropionitrile) (AIBN), ethanol (EtOH), tetra-
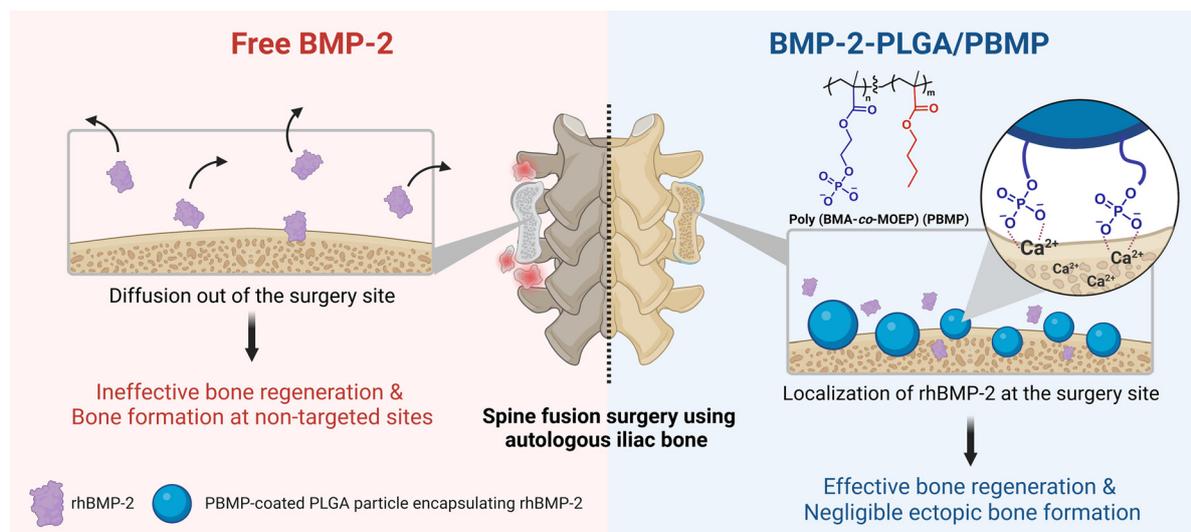

Fig. 1 Schematic illustration of applying BMP-2-PLGA/PBMP microparticles to the spine fusion surgery with autologous iliac bone (AIB) for the localized delivery and enhanced therapeutic effect of rhBMP-2.

hydrofuran (THF), fluorescein, bovine serum albumin (BSA), and sodium dodecyl sulfate (SDS) were purchased from Sigma Aldrich (St Louis, MO, USA). Polyvinyl alcohol (PVA) (average M_w = 13 000–23 000) and dimethyl chlorophosphate (DCP) were purchased from Acros Organics (Geel, Belgium). Bromotrimethylsilane (TMSBr) was purchased from TCI (Tokyo, Japan). Dichloromethane (DCM), methanol (MeOH), and dimethyl sulfoxide (DMSO) were purchased from Samchun (Seoul, Korea). rhBMP-2 was donated from CGBio (Seoul, Korea). A p-nitrophenyl phosphate (pNPP) alkaline phosphatase assay kit was purchased from Anaspec (CA, USA). Anti-RUNX2 antibody (F-2) and Anti-ALP antibody (A-10) were acquired from Santa Cruz Biotechnology (TX, USA). Goat anti-mouse Alexa Fluor 488 was purchased from Abcam (Cambridge, UK).

2.2 Synthesis and characterization of PBMP

PBMP was synthesized as previously reported.[23,24] In brief, DCP (0.15 mmol) and pyridine (0.15 mol) were mixed and slowly added into 10 mL of chloroform containing HEMA (0.10 mol). The mixture was stirred for 3 h at ambient temperature and washed with 0.01 M HCl. After evaporating the washed organic layer, dimethyl methacryloyloxyethyl phosphate (DMOEP) was obtained. For the polymerization, DMOEP (0.10 mol) and BMA (0.10 mol) monomers were added to an EtOH/THF (v/v = 8/2) mixture with AIBN (0.0020 mol) as an initiator. After an overnight polymerization at 60 °C, poly(BMA-co-DMOEP) was obtained. After the evaporation of the solvent, the polymer was dissolved in anhydrous chloroform. Ice-cold TMSBr (0.25 mol) was slowly added to the solution and stirred for 3 h at ambient temperature. After the evaporation of the solvent, a water/THF (v/v = 1/7) mixture was added. After stirring overnight at ambient temperature, the deprotected polymer was purified using a dialysis membrane (Spectrum Laboratories, MWCO = 3 kDa) against deionized water. PBMP was obtained as a white powder after freeze-drying. The overall yield was over 60%. Gel Permeation Chromatography (GPC) was used for the characterization of PBMP.

2.3 Preparation of PLGA and PLGA/PBMP microparticles

Microparticles encapsulating rhBMP-2 were prepared by a previously reported water-in-oil-in-water (w/o/w) double emulsion method with slight modification. rhBMP-2 was dissolved in purified water at a concentration of 0.1% (w/v) and PLGA was dissolved in DCM at a concentration of 5.0% (w/v) separately. The rhBMP-2 solution was dispersed in the PLGA solution with rapid homogenization at 3000 rpm for 1 min to form a water-in-oil (w/o) primary emulsion. The primary emulsion was added into an aqueous solution of PVA (2 mL) at a concentration of 3.0% (w/v) followed by the same homogenization step to form a water-in-oil-in-water (w/o/w) double emulsion. The emulsion was stirred with a magnetic stirrer for 5 h at 37 °C to evaporate DCM. After solvent evaporation, the resulting dispersion was added into 20 mL of an aqueous PVA solution (0.3% w/v) and stirred for an additional 1 h to obtain PLGA microparticles encapsulating rhBMP-2 (BMP-2-PLGA).

For PBMP-coated PLGA microparticles (BMP-2-PLGA/PBMP), the dispersion obtained after the 5 h stirring step was instead transferred into a 0.3% (w/v) PVA solution containing PBMP (0.1% w/v) and further stirred for 1 h. The resulting particle suspension was centrifuged (Supra 21K, Hanil, Korea) at 8000 rpm for 5 min and resuspended in deionized water. After repetitive washing (×3) with deionized water, the particles were lyophilized. Microparticles encapsulating BSA were fabricated by the same procedure using BSA instead of rhBMP-2. Microparticles encapsulating fluorescein were fabricated using an oil-in-water (o/w) single emulsion method using 200 μg of fluorescein in a DCM/DMSO (v/v = 8/2) mixture as an oil phase and 3.0% (w/v) PVA as an aqueous phase as previously reported.[24]

2.4 Characterization of PLGA and PLGA/PBMP microparticles

The morphologies of the PLGA and PLGA/PBMP particles were examined by field-emission scanning electron microscopy (FE-SEM) (SIGMA; Carl Zeiss, Jena, Germany) after coating with Pt by a sputter (EM ACE200; Leica, Wetzlar, Germany). The zeta potential of the prepared particles was measured using a Zetasizer (Zetasizernano ZS; Malvern, UK). The amount of rhBMP-2 and BSA in the PLGA and PLGA/PBMP microparticles was determined using a BCA protein assay kit (Thermo Scientific, MA, USA). Briefly, 1.0 mg of the particles was completely dissolved in 20 μL of DMSO, followed by the addition of 80 μL of 0.05 M NaOH with 0.5% (w/v) of SDS. The samples were then centrifuged at 13 000 rpm for 2 min. 10 μL of the supernatant was collected from each sample for the quantification of the protein amount by BCA assay. The drug content and the encapsulation efficiency were calculated as follows.

$$\text{Drug content} \ (\mu g \ mg^{-1}) = \frac{\text{mass of drug loaded in particles}}{\text{mass of particles}}$$

$$\text{Encapsulation efficiency} \ (\%) = \frac{\text{mass of drug loaded in particles}}{\text{mass of drug in the preparation solution}} \times 100$$

2.5 In vitro protein release from PLGA and PLGA/PBMP microparticles

The release of proteins from the particles was analysed by the sample and separation method. The BSA release was evaluated for 8 weeks, while rhBMP-2 release was evaluated for 4 weeks. Microparticles encapsulating proteins were prepared at a concentration of 10 mg mL^{-1} in PBS. The suspension was stirred with a magnetic stirrer at 37 °C. At each time point, 200 μL of the solution was sampled and centrifuged at 14 000 rpm for 10 min. The supernatant was collected for the quantitative analysis of the released amount by the BCA assay. The release of BSA and rhBMP-2 was quantified using BSA and rhBMP-2 as the standards, respectively.

2.6 Cell culture

Mouse preosteoblast (MC3T3-E1) cells were cultured in α-MEM supplemented with 100 U mL^{-1} penicillin, 100 μg mL^{-1} strep-

tomycin, and 10% fetal bovine serum (FBS). The cells were maintained at 37 °C under a humidified atmosphere containing 5% CO_2. Osteogenic medium was prepared by the addition of 10 mM β-glycerophosphate and 50 μg mL^{-1} ascorbic acid to the culture medium.

2.7 *In vitro* bioactivity of released rhBMP-2

The bioactivity of rhBMP-2 released from the microparticles was assessed using an alkaline phosphatase (ALP) activity assay. Free rhBMP-2 (10 μg mL^{-1}) or rhBMP-2-loaded PLGA/PBMP microparticles (10 mg mL^{-1}, with a total rhBMP-2 concentration of 6.0 μg mL^{-1}) were incubated in PBS at 37 °C for 1 and 24 h. After incubation, free rhBMP-2 or the eluates from microparticles were collected and centrifuged at 14 000 rpm for 10 min. The supernatant was diluted to a final rhBMP-2 concentration of 100 ng mL^{-1} in osteogenic medium. MC3T3-E1 cells were seeded in 24-well plates at a density of 1×10^4 cells per well and treated with osteogenic medium containing free rhBMP-2 or eluted rhBMP-2 (100 ng mL^{-1}) for 7 days, with medium exchanges every 3 days. To evaluate the particles' intrinsic biological effect, empty PLGA/PBMP microparticles (10 mg mL^{-1}) were also incubated for 1 h and processed using the same procedure. ALP activity was subsequently quantified using a pNPP alkaline phosphatase assay kit (Anaspec, CA, USA). The measured enzyme activity was normalized to the total cellular protein content, which was determined using a BCA assay.

2.8 Bone-binding affinity of microparticles

The calcium-binding affinity of PLGA and PLGA/PBMP microparticles was evaluated by measuring the fluorescence intensity of fluorescein-encapsulated microparticles bound to rat femurs. Briefly, rat femur samples were immersed in a suspension of PLGA or PLGA/PBMP microparticles (5 mg mL^{-1} in deionized water) for 10 min. After immersion, the samples underwent repetitive washing steps and were dried in a vacuum oven overnight. The particle-bound bone samples were then immersed in DMSO for 15 min to completely dissolve the microparticles, followed by the addition of an equal volume of PBS. The fluorescence of the resulting eluates was measured using a microplate reader at an excitation/emission wavelength of 485/525 nm to quantify the number of adhered particles on the bone surface.

2.9 Analysis of osteogenesis markers in MC3T3-E1 cells

2.9.1 Coating of hydroxyapatite discs with microparticles.
To coat hydroxyapatite (HA) discs with microparticles, BMP-2-PLGA or BMP-2-PLGA/PBMP microparticles were suspended in deionized water at a concentration of 20 mg mL^{-1}. The HA discs were immersed in the suspension for 1 min at ambient temperature, washed thoroughly three times with deionized water, and subsequently dried in an oven at 37 °C overnight.

2.9.2 RT-qPCR analysis.
Microparticle-coated HA discs were incubated in PBS at 37 °C for 10 days to facilitate the release of rhBMP-2. The resulting solution was collected and centrifuged at 14 000 rpm for 10 min to remove any residual

particles. MC3T3-E1 cells were seeded in 24-well plates at a density of 2.5×10^4 cells per well and cultured in a 1 : 1 mixture of osteogenic medium and the collected solution containing released rhBMP-2. After incubation for 2 days, half of the medium was replaced with a fresh mixture of osteogenic medium and the collected rhBMP-2 solution. After further incubation for 2 days, total RNA was extracted from the cells using a Total RNA Miniprep kit (Enzynomics, Daejeon, Korea). The purified RNA was then used for cDNA synthesis with a TOPscript™ cDNA synthesis kit (Enzynomics, Daejeon, Korea). RT-qPCR was performed using TOPreal™ SYBR Green qPCR UDG PreMIX (Enzynomics, Daejeon, Korea) according to the manufacturer's protocol. The primers used for RT-qPCR analysis are listed in Table S1. *Gapdh* was used as the housekeeping gene for normalization.

2.9.3 Immunocytochemical analysis.
MC3T3-E1 cells were seeded directly onto microparticle-coated HA discs in a 24-well plate at a density of 4×10^4 cells per well and cultured in osteogenic medium. After incubation for 2 days, half of the medium was replaced with fresh osteogenic medium. After further incubation for 2 days, the HA discs were gently washed with PBS, and the cells were fixed with 4% (w/v) paraformaldehyde (PFA) for 15 min. The cells were then permeabilized with 0.1% (v/v) Triton X-100 for 5 min and blocked with 3% BSA in 0.1% (v/v) Triton X-100 for 1 h. Subsequently, the cells were incubated with a primary antibody against RUNX2 (1 : 100, Santa Cruz) or ALP (1 : 100, Santa Cruz) at 4 °C for 16 h. After washing, the cells were treated with a goat anti-mouse Alexa Fluor 488 secondary antibody (1 : 400, Abcam) for 1 h in the dark. Finally, nuclei were counterstained with Hoechst 33342 (1 : 1000 dilution) for 5 min. Fluorescence images were acquired using a Zeiss LSM 980 confocal microscope (Zeiss, Oberkochen, Germany).

2.10 *In vivo* bone formation after posterolateral spine fusion in a rat model

2.10.1 Animals.
The animal experiment was performed according to the recommendations of the Guide for the Care and Use of Laboratory Animals of the National Institutes of Health. The protocol was approved by the Institutional Animal Care and Use Committee of the Clinical Research Institute, Seoul National University Hospital, Seoul, Korea (permit number: 14-0259-C1A0).

Ten-week-old male Sprague-Dawley rats obtained from Orient Bio (Gyonggi, Korea) were used and housed singly in a pathogen-free ventilated cage with a 12 hour light/dark cycle. The rats were allowed free access to tap water and standard rodent chow (Cargill, Gyonggi, Korea) that contained 1.35% (w/w) calcium and 0.44% (w/w) phosphate and no vitamin D.

2.10.2 *In vivo* experimental design and surgery.
After 2 weeks of acclimatization, 40 ten-week-old male Sprague-Dawley rats were divided into five groups ($n = 10$ each, except $n = 5$ for BMP(0.5)-PLGA/PBMP and BMP(5)-PLGA/PBMP): control (autologous iliac bone (AIB)), free BMP(5) (AIB + collagen soaked with 5 μg rhBMP-2), BMP(0.5)-PLGA/PBMP (AIB + PLGA/PBMP particles containing 0.5 μg rhBMP-2), BMP(2.5)-

PLGA/PBMP (AIB + PLGA/PBMP particles containing 2.5 μg rhBMP-2), and BMP(5)-PLGA/PBMP (AIB + PLGA/PBMP particles containing 5 μg rhBMP-2). All rats underwent unilateral posterolateral intertransverse fusion with AIB. Anesthesia was induced with 5% isoflurane and maintained with 2.5% isoflurane; during the maintenance, oxygen was supplied through a coaxial nose cone. A posterior midline incision was made over the spinous process on L4–L5. After the left-side dorsal incision, the L4 and L5 transverse processes were exposed by muscle splitting between the multifidus and erector spinae muscles. The cortical bone of the transverse processes of L4 and L5 was decorticated with an electronic bur, and about 0.25 g of AIB was harvested from the ipsilateral iliac bone. The AIB mixed with PLGA/PBMP particles containing rhBMP-2 at the dose according to each group was placed between the decorticated transverse processes of L4 and L5.

2.10.3 Evaluation of bone formation. Rats in each group were euthanized at 4 and 8 weeks after fusion surgery, respectively. Three-dimensional (3-D) micro-CT was performed (NFR-Polaris-G90, NanoFocusRay, Jeonbuk, Korea) for the assessment of bone formation. Scans were performed initially from the lower end plate of the S2 vertebral body and proceeded cranially; the images, including 720° views, were acquired at 70 kVp, 80 A, and 100 ms per frame. Total 512 slices were acquired with a reconstructed image size of 1024 × 1024 pixels and a voxel size of 56 × 56 × 124 μm.[3] The axial images were converted to 3-D images using Digital Imaging and Communications in Medicine (DICOM) software (Lucion, Infinite Healthcare, Seoul, Korea). The volume between the upper end plate of L4 and the lower end plate of L5 including the volume of the applied AIB was measured with a threshold of >700.

In each group, the bone volume change during weeks 0–4 was calculated by subtracting the average bone volume at week 0 from the bone volume of each animal sacrificed at week 4. Similarly, the bone volume change during weeks 4–8 was determined by subtracting the average bone volume at week 4 from the bone volume of each animal sacrificed at week 8. It is important to note that these values do not represent longitudinal measurement of the same subjects over time, but rather reflect group-wise comparisons at distinct time points. Ectopic bone formation was defined as the bone formation outside the parts between L4 and L5 transverse processes, which were the original spinal fusion sites. The presence or absence of ectopic bone formation was evaluated by micro-CT.

2.10.4 Histological evaluation of *in vivo* bone formation after posterolateral spine fusion. Samples including the L4–L5 intertransverse processes and adjacent vertebral bodies were harvested and fixed with 4% paraformaldehyde. The specimens were decalcified in 5% nitric acid for 3 days, washed in distilled water, and embedded in paraffin. Unilateral sagittal sections with a thickness of 5 μm were obtained from the midline of the intertransverse process area. The sections were stained with Alcian blue and Masson's trichrome with hematoxylin/fast green and observed using light microscopy. We compared the stained areas to analyse the new bone formation at the spine fusion site.

2.11 Statistical analysis

We performed all the quantitative experiments at least in triplicate. The data are expressed as mean value ± standard deviation. Statistical significance was determined by two-tailed Student's *t*-test, one-way analysis of variance (ANOVA) after Bonferroni's correction, and Fisher's exact test using GraphPad Prism software (5.0; GraphPad, San Diego, CA, USA). A *p*-value less than 0.05 was considered significant.

3. Results and discussion

3.1 Synthesis of PBMP

Poly(BMA-*co*-MOEP) (PBMP), which was designed to enhance the binding affinity of drug-loaded PLGA particles towards calcium-rich surfaces, was synthesized by free radical polymerization using BMA and DMOEP as monomers based on the previously reported procedures.[23] Hydrophobic *n*-butyl groups in BMA are expected to interact with the hydrophobic surface of the PLGA particle, while phosphomonoester groups in MOEP provide strong affinity towards the calcium-bearing materials, such as bones. ^{1}H NMR spectra showed successful synthesis of PBMP, with the BMA : MOEP ratio of 60 : 40 in the polymer (Fig. S1A). GPC analysis showed the number average molecular weight (M_n) of 16 900 g mol^{-1} and the weight average molecular weight (M_w) of 32 200 g mol^{-1} (Fig. S1B), which are below the cut-off values of the excretion in the kidneys.[25] The dispersity ($Đ$) of 1.91 was a typical characteristic of polymers synthesized by free radical polymerization.

3.2 Encapsulation of rhBMP-2 in PLGA and PLGA/PBMP microparticles

For the encapsulation of rhBMP-2 into the PLGA particles, we used the water-in-oil-in-water (w/o/w) emulsion/evaporation method, which is well-known for the fabrication of PLGA microparticles encapsulating hydrophilic proteins.[26,27] PLGA microparticles could be coated with PBMP by incubation in a PBMP-dissolved solution. The resulting particles were examined with FE-SEM, showing spherical shapes with an average diameter of around 0.7 μm (Fig. 2 and Table 1). Non-coated PLGA particles exhibited a slightly negative zeta potential (−8.14 mV) due to the carboxylate end groups of the PLGA
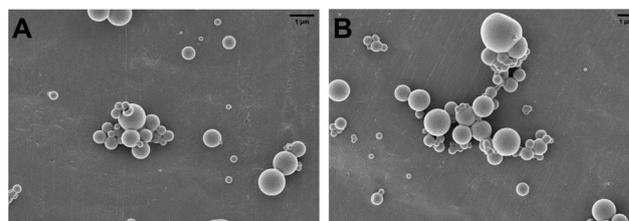

Fig. 2 Preparation of rhBMP-2-loaded PLGA microparticles with or without PBMP coating. FE-SEM images of non-coated PLGA microparticles (BMP-2-PLGA) (A) and PBMP-coated PLGA microparticles (BMP-2-PLGA/PBMP) (B).

Table 1 Characterization of BMP-2-PLGA and BMP-2-PLGA /PBMP microparticles. The particle size was measured by the analysis of the particles ($n > 400$) in FE-SEM images. The values in the zeta potential, drug content and loading efficiency were obtained in three independent experiments ($n = 3$). All values are indicated as the mean $\pm$ S.D

Microparticles	Size (μm)	Zeta potential (mV)	rhBMP-2 loading	
			Content (μg mg^{-1})	Encapsulation efficiency (%)
BMP-2-PLGA	0.70 ± 0.41	−8.14 ± 2.69	0.68 ± 0.47	27.1 ± 19.0
BMP-2-PLGA/PBMP	0.68 ± 0.35	−27.18 ± 3.27	0.58 ± 0.21	23.0 ± 1.6

backbone. On the other hand, PLGA/PBMP microparticles exhibited a much lower zeta potential (−27.18 mV), which was attributed to the negatively charged phosphomonoester groups in the side chains of PBMP. The result implied that PBMP could be coated on the surface of PLGA microparticles successfully.

The loaded amount of rhBMP-2 in the fabricated particles was measured by BCA assay. PLGA and PLGA/PBMP particles showed protein contents of 0.68 μg mg^{-1} and 0.58 μg mg^{-1}, respectively. The encapsulation efficiency was calculated as 27.1% and 23.0% for PLGA and PLGA/PBMP particles, respectively. Overall, the results confirmed that the PBMP-coating on the PLGA particle surface did not significantly influence the morphology nor the protein loading of the particles.

3.3 *In vitro* protein release from PLGA and PLGA/PBMP microparticles

The release of encapsulated proteins from PLGA and PLGA/PBMP microparticles was measured by BCA assay. Initially, bovine serum albumin (BSA) was employed as a model protein to compare the release behaviour of PLGA and PLGA/PBMP microparticles. The cumulative release profiles of BSA from particles are presented as solid lines in Fig. 3. Both PLGA and PLGA/PBMP showed burst release up to 20% within the initial 1 h of incubation possibly due to the rapid diffusion of weakly bound BSA around the particle surface. Subsequently, BSA was released from the particles in a sustained manner for up to 8 weeks. PLGA/PBMP particles showed cumulative release of 37% and 45% on days 7 and 14, reaching around 50% after 4

weeks. By the time point of 8 weeks, a total of 76% of encapsulated BSA was released from PLGA/PBMP. The protein release profiles of PLGA and PLGA/PBMP are quite similar to each other. The release rate from PLGA/PBMP was slightly faster than that from PLGA, but the difference was not statistically significant. PBMP coating seems to have a minimal effect on the protein release from the PLGA-based microparticles.

The release of the therapeutic protein rhBMP-2 from PLGA/PBMP microparticles was also quantified using a BCA assay with rhBMP-2 as the standard. Similar to the release pattern observed from BSA, an initial burst release of approximately 20% occurred within the first hour, followed by gradual and sustained release reaching 28% and 43% by days 7 and 14, respectively, and reaching 60% by week 4 (Fig. S2). This prolonged release kinetic is highly desirable for bone healing, a process that requires maintaining therapeutic concentration over several weeks. We envisioned that the PLGA/PBMP system can provide localized, long-term delivery of rhBMP-2, potentially avoiding the systemic side effects associated with high-dose treatments.

3.4 Retention of rhBMP-2 bioactivity in PLGA/PBMP microparticles

Assessing the bioactivity of encapsulated proteins is crucial, as the fabrication process can potentially lead to protein denaturation. To evaluate whether rhBMP-2 retained its osteoinductive activity following encapsulation in PLGA/PBMP microparticles, we conducted a comparative analysis. Specifically, rhBMP-2 was released from BMP-2-PLGA/PBMP by incubation in PBS at 37 °C, and its osteoinductive activity was compared with that of free rhBMP-2 incubated under the same conditions. It was confirmed that the osteoinductive activity of free rhBMP-2 was not significantly decreased under the incubation conditions.

Alkaline phosphatase (ALP) activity, which is a key indicator of osteogenesis, was measured in preosteoblast MC3T3-E1 cells after 7 day treatment with each rhBMP-2 sample at an equal concentration (100 ng mL^{-1}). The possible toxicity of PLGA/PBMP microparticles was examined in a previous study using the same cell line, showing no significant cytotoxicity up to 1000 μg mL^{-1}.[23]

As shown in Fig. 4, rhBMP-2 released from BMP-2-PLGA/PBMP exhibited no significant difference in ALP activity compared to free rhBMP-2 after 1 h-incubation, indicating that the encapsulation process did not compromise its osteoinductive function. Notably, rhBMP-2 released from BMP-2-PLGA/PBMP
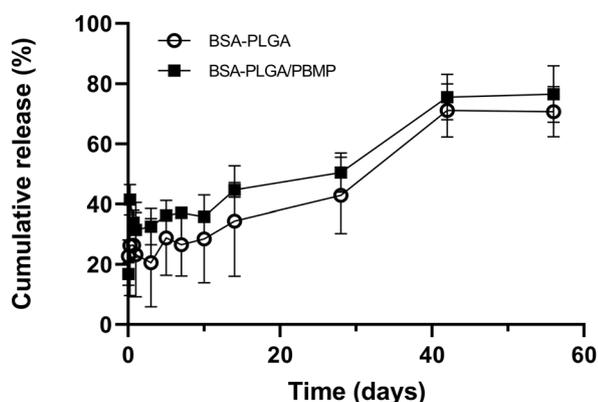

Fig. 3 *In vitro* release of BSA as a model protein from PLGA and PLGA/PBMP microparticles. All values are indicated as the mean ± S.D ($n = 3$).
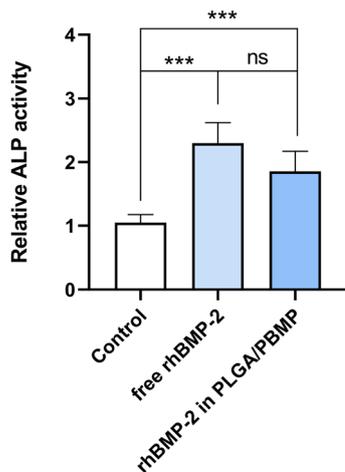
Fig. 4 *In vitro* bioactivity of rhBMP-2 released from the PLGA/PBMP microparticles determined by alkaline phosphatase (ALP) activity in MC3T3-E1 cells. Eluates were collected after incubating microparticles in PBS for 1 h at 37 °C. The cells were then treated with the eluates which were diluted to a final rhBMP-2 concentration of 100 ng mL^{-1}, for 7 days before ALP quantification. ALP activity was normalized to that of the control group. The error bar represents the standard deviation. The statistical analysis was performed using one-way analysis of variance (ANOVA). *** indicates $p < 0.001$. ns means not significant.

Fig. 5 *Ex vivo* bone binding of PLGA and PLGA/PBMP microparticles. Fluorescein-loaded PLGA and PLGA/PBMP microparticles were used for the measurement of bone binding. The fluorescence intensity was measured by dissolving all the adhered-particles on the surface of bone samples. The error bar represents the standard deviation of the measurements. The statistical analysis was performed using Student's unpaired *t*-test. * indicates $p < 0.05$.

retained its bioactivity and induced two-fold higher ALP activity compared to the control group even after 24 h-incubation (Fig. S3). This result suggests that PLGA/PBMP microparticles can serve as a protective carrier, effectively shielding rhBMP-2 from deactivation. Such protection is advantageous for maintaining long-term therapeutic efficacy *in vivo*, ultimately contributing to successful bone regeneration. Empty PLGA/PBMP microparticles did not exhibit any induction of ALP activity compared to the control group (Fig. S4).

3.5 Bone-binding affinity of PLGA and PLGA/PBMP microparticles

One of the major drawbacks of using BMP-2 in the clinic is unfavourable ectopic bone formation.[10,28] Therefore, it is very crucial to maintain the concentration of BMP-2 only around the target site by preventing the leakage or diffusion of BMP-2 to non-targeted areas. We expected that calcium-binding PBMP coating on the PLGA particle surface would greatly enhance the binding affinity towards the calcium-rich surface, owing to its phosphomonoester groups. As shown in their outstanding binding affinity onto hydroxyapatite[29] or exposed bones in the sinonasal cavity after surgery,[24] PLGA/PBMP microparticles could have strong binding affinity to the target bone during bone surgery and minimize the release of rhBMP-2 at unwanted sites.

To compare the binding affinity of non-coated PLGA particles and PLGA/PBMP particles to bones, we prepared fluorescein-loaded particles and measured the fluorescence intensity on the surface of sliced rat femurs *ex vivo* (Fig. 5). The results revealed that bone samples immersed with PLGA/PBMP particles showed approximately 2 times higher fluo-
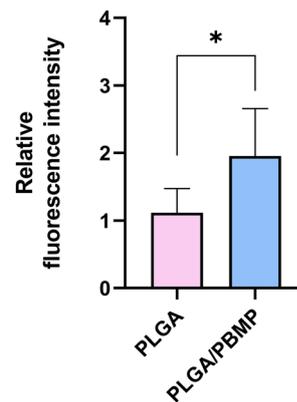
rescence intensity than bare PLGA particles, even after repetitive washing procedures for releasing weakly bound particles. Although non-coated PLGA can interact with bones to some extent probably due to the interaction between calcium in bones and carboxylate in PLGA, it is reported that the interaction between calcium ions and phosphomonoester is much stronger.[30] Based on the result of the *ex vivo* binding analysis, we could presume that the administered PLGA/PBMP particles would strongly adhere to the bone surfaces in the surgical lesion, allowing rhBMP-2 to be released in the target area.

3.6 *In vitro* osteogenesis induced by BMP-2-PLGA and BMP-2-PLGA/PBMP

As shown in Fig. 5, the PBMP coating was designed to enhance the binding affinity of PLGA microparticles to bone surfaces. We therefore expected that this increased adhesion would lead to greater particle retention on bone surfaces compared to that of uncoated PLGA particles, thereby elevating the local concentration of rhBMP-2 near the adhesion sites and promoting osteogenic differentiation.

To simulate the osteogenic process *in vitro*, hydroxyapatite (HA) discs were coated with either BMP-2-PLGA or BMP-2-PLGA/PBMP particles and incubated in PBS for 10 days to collect released rhBMP-2. These eluates were subsequently used to induce osteogenesis in MC3T3-E1 preosteoblasts. As shown in Fig. 6A, the transcription levels of Runt-related transcription factor 2 (*Runx2*) were measured by RT-qPCR after a 5 day treatment with the collected eluates.[31–33] While the BMP-2-PLGA group showed a minimal difference from the control, the BMP-2-PLGA/PBMP group exhibited a 2.3-fold increase in *Runx2* expression relative to the control.

To further assess osteogenic potential in a more biomimetic setting that simulates localized cell-particle interactions, MC3T3-E1 cells were directly seeded onto the particle-coated
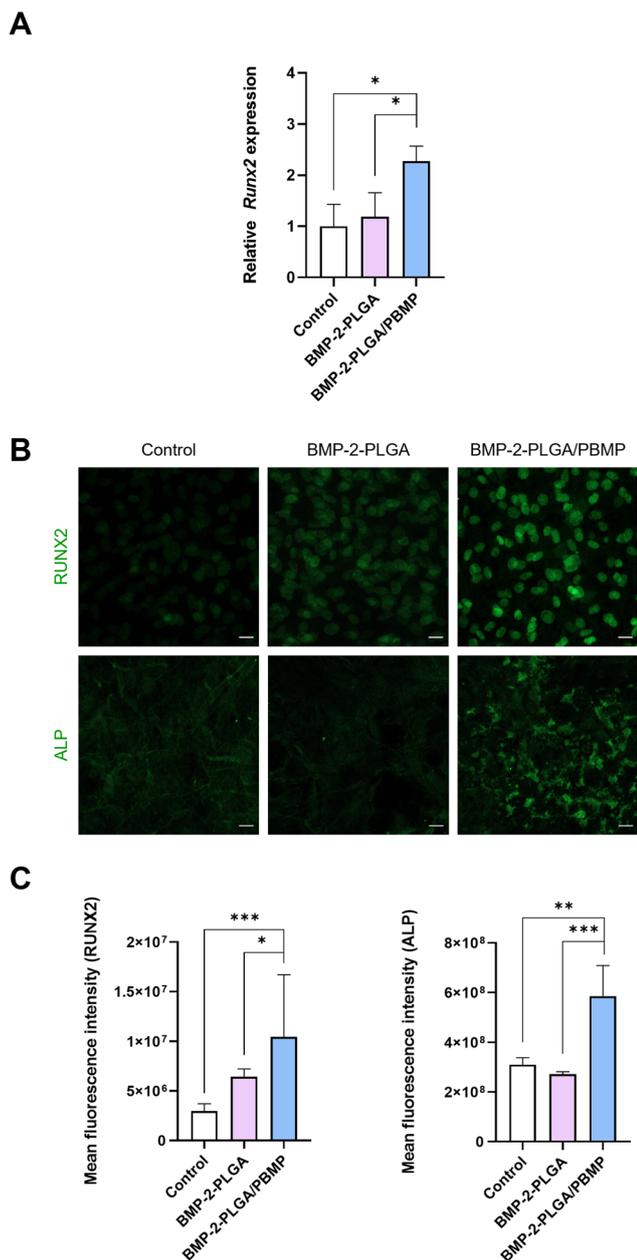
A

chosen because early osteogenic markers reach their peak between days 3 and 7.[36,37] Confocal laser scanning microscopy (CLSM) images revealed markedly higher expression of RUNX2 and ALP in cells cultured on HA discs coated with BMP-2-PLGA/PBMP particles compared to both the control and BMP-2-PLGA groups (Fig. 6B). Quantitative analysis confirmed that the BMP-2-PLGA/PBMP group displayed 1.6-fold and 2.2-fold higher expression of RUNX2 and ALP, respectively, than the BMP-2-PLGA group (Fig. 6C).

Collectively, the significantly elevated expression of both osteogenic markers supports the notion that the PBMP-coated particles enhance retention at the bone surface, thereby maintaining a sufficient local concentration of rhBMP-2 to effectively promote osteogenesis. These findings highlight the potential of our delivery system to facilitate robust osteoprogenitor cell differentiation and underscore its promise for improving bone regeneration *in vivo*.

3.7 Evaluation of bone formation after posterolateral spine fusion

To evaluate the bone formation efficacy of rhBMP-2 released from PLGA/PBMP microparticles, we used the posterolateral spinal fusion surgery model using rats mimicking the clinical practice in the present and previous studies.[38,39] In the model, unilateral fusion surgery was performed, with the contralateral non-operated side serving as an internal control to enable accurate evaluation of bone formation. AIB was harvested from the rat and applied with vehicles containing rhBMP-2. PLGA/PBMP microparticles encapsulating rhBMP-2 were prepared for the binding on the AIB surface (Fig. 7). The AIB treated with free rhBMP-2 at a dose of 5 μg (free BMP(5)) or PLGA/PBMP encapsulating rhBMP-2 (BMP(5)-PLGA/PBMP, BMP(2.5)-PLGA/PBMP, and BMP(0.5)-PLGA/PBMP) at various doses of rhBMP-2 (5 μg, 2.5 μg and 0.5 μg doses per rat) was placed over the spinous processes on L4–L5 for facilitating intertransverse
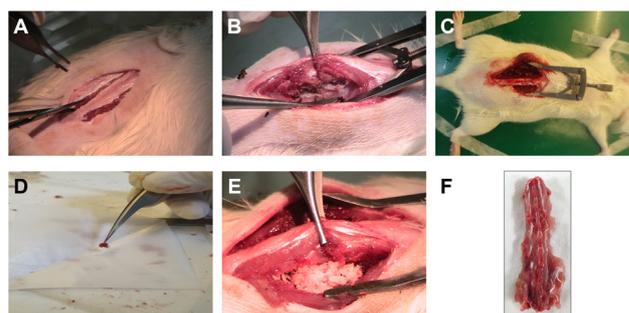
B

C

Fig. 6 Analysis of osteogenic markers in MC3T3-E1 cells cultured with rhBMP-2 released from HA disc bound microparticles. (A) RT-qPCR analysis of *Runx2* expression. Cells were stimulated for 5 days with a conditioned buffer obtained by a 10 day incubation of the HA disc coated with microparticles. Gene expression was normalized to *Gapdh*. (B) Representative confocal microscopy images of cells incubated on the microparticle-coated HA discs for 5 days. RUNX2 and ALP are stained in green. The scale bar represents 20 μm. (C) Quantification of the fluorescence signal for RUNX2 and ALP in cells incubated on the microparticle-coated HA discs. The error bar represents the standard deviation. The statistical analysis was performed using one-way analysis of variance (ANOVA). *, **, and *** indicate $0.01 \leq p < 0.05$, $0.001 \leq p < 0.01$ and $p < 0.001$, respectively. *ns* means not significant.

Fig. 7 *In vivo* experimental process of posterolateral intertransverse fusion with autologous iliac bone (AIB) in a rat model. (A) Midline incision of the back skin over the spine and dissection of spinae muscle. (B) Exposure of transverse processes of L4 and L5 to be operated on. (C) Exposure and harvest of the ipsilateral iliac bone for AIB. (D) Applying BMP-2-PLGA/PBMP microparticles on the surface of AIB. (E) Placing the mixture of AIB and BMP-2-PLGA/PBMP microparticles in between the decorticated transverse process of L4 and L5. (F) After 4 and 8 weeks of the surgery, half of each group is euthanized for micro-CT scanning and histological analysis.

HA discs. After 5 days of culture, the expression levels of key osteogenic markers, RUNX2 and ALP, were examined by immunocytochemistry (ICC).[33–35] The 5 day time point was

fusion. The dose was selected based on previous posterolateral spinal fusion studies demonstrating robust and effective fusion at a rhBMP-2 dose of 2–10 μg per rats.[40,41] At the time point of 4 and 8 weeks after the surgery, half of each group was sacrificed for micro-CT scanning and histological staining of the spine bones. The 4 and 8 week time points were selected to assess initial osteogenic activity and mature bone remodelling based on previously established fusion model timelines. We reported that a rat in the free BMP(5) group and a rat in the control group died 2 weeks and 6 weeks after the fusion surgery, respectively.

The micro-CT images of the harvested spine bones are shown in Fig. 8A. The bone volume change between each time point was calculated from the micro-CT data and is plotted in Fig. 8B and C. Without any rhBMP-2 treatment (control), the volume of the fusion bed increased by 51 mm^3 between 0 and 4 weeks after the AIB surgery, but slightly decreased between 4 and 8 weeks. In bone remodelling using harvested auto- or allobone, the grafted bone on the fusion bed is gradually absorbed over time and becomes matured.[42,43] Therefore, if osteoinductive materials are not released until the late stage of bone remodelling, the volume of the bone on the fusion bed decreases. In contrast, if the osteoinductive materials are released until the late stage of bone remodelling, the absorption of the grafted bone can be reduced or the bone volume on the fusion bed can increase. When free BMP(5) was administered at a dose of 5 μg, the bone volume increased by 126 mm^3 from 0 to 4 weeks, which is the largest change among all groups. This suggests a rapid and strong osteoinduction by rhBMP-2 in the fusion bed. However, there was no significant change in bone volume between 4 and 8 weeks, implying minimal activity of rhBMP-2 in this period.

On the other hand, groups treated with BMP(0.5)-PLGA/PBMP or BMP(2.5)-PLGA/PBMP showed almost no significant change in bone volume between 0 and 4 weeks (Fig. 8B). The group treated with BMP(5)-PLGA/PBMP showed a decrease in bone volume during this period possibly due to the absorption of the grafted bone. However, from 4 to 8 weeks, the increase

of the bone volume was observed in a dose-dependent manner (Fig. 8C). Although BMP(0.5)-PLGA/PBMP showed minimal changes in bone volume, BMP(2.5)-PLGA/PBMP and BMP(5)-PLGA/PBMP showed a significant increase in bone volume by 56 mm^3 and 63 mm^3, respectively. Unlike other groups with negligible bone volume changes, only these two groups showed a significant increase in bone volume in the period between 4 and 8 weeks.

The distinctive osteogenic effect of free BMP(5) and BMP-PLGA/PBMP reflected the significance of the sustained release behaviour of rhBMP-2 from PLGA/PBMP microparticles. Free rhBMP-2 gave a rapid osteogenic effect in the early period between 0 and 4 weeks but the effect diminished in the late period between 4 and 8 weeks, probably due to rapid diffusion from the spine fusion surgery site and elimination from the body. On the other hand, encapsulated protein drugs can be released in a sustained manner from PLGA/PBMP microparticles for more than 6 weeks, as shown in Fig. 3. Therefore, PLGA/PBMP could release encapsulated rhBMP-2 in a sustained manner to start facilitating the bone growth more slowly and to maintain the effective concentration for osteogenesis around the attached bone surfaces until the late period from 4 to 8 weeks.

The dose–efficacy relationship could also be obtained from the results. While PLGA/PBMP microparticles can release rhBMP-2 nearby the administered site for a prolonged period, the concentration of rhBMP-2 might not be maintained over the threshold value for the osteoinduction if the dosage of rhBMP-2 encapsulated in PLGA/PBMP is too low. BMP(0.5)-PLGA/PBMP, which contains only 0.5 μg of rhBMP-2, showed an almost minimal effect on osteoinduction. When the dosage of rhBMP-2 was 2.5 μg or 5 μg, PLGA/PBMP microparticles induced gradual osteogenesis up to 8 weeks. BMP(2.5)-PLGA/PBMP, which contains only half the amount of rhBMP-2 compared to free BMP(5), could maintain the osteogenic activity even 8 weeks after following the spinal surgery.

The new bone formation was also observed in the stained images of the harvested bone tissues (Fig. 9A). The Alcian blue
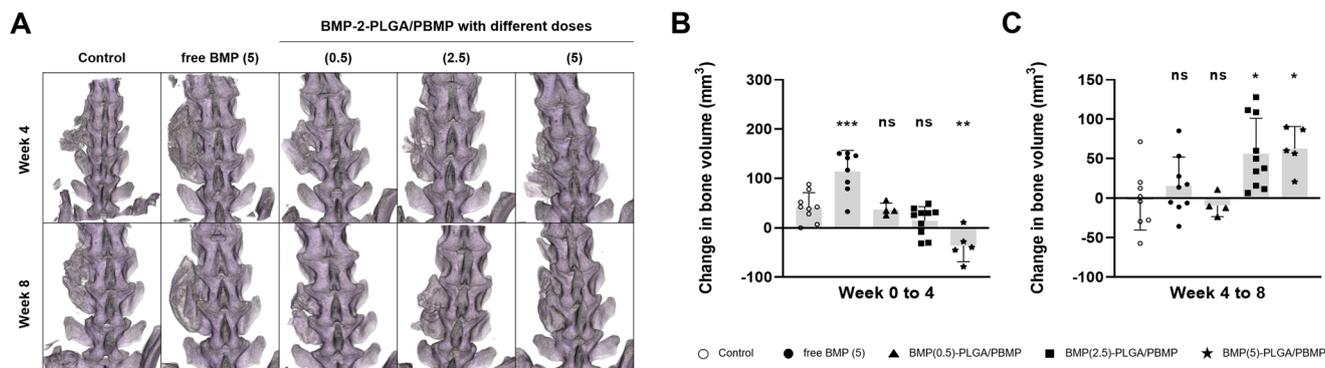

Fig. 8 Evaluation of bone formation in the spine after the spine fusion surgery in the rat model. (A) Representative micro-CT images of transverse processes with bone formation after 4 and 8 weeks of spinal fusion surgery. The bone volume change from week 0 to 4 (B), and from week 4 to 8 (C) in the micro-CT images. The error bar represents the standard deviation. The statistical analysis was performed using one-way analysis of variance (ANOVA). *, **, and *** indicate $0.01 \leq p < 0.05$, $0.001 \leq p < 0.01$ and $p < 0.001$, respectively. ns means not significant.
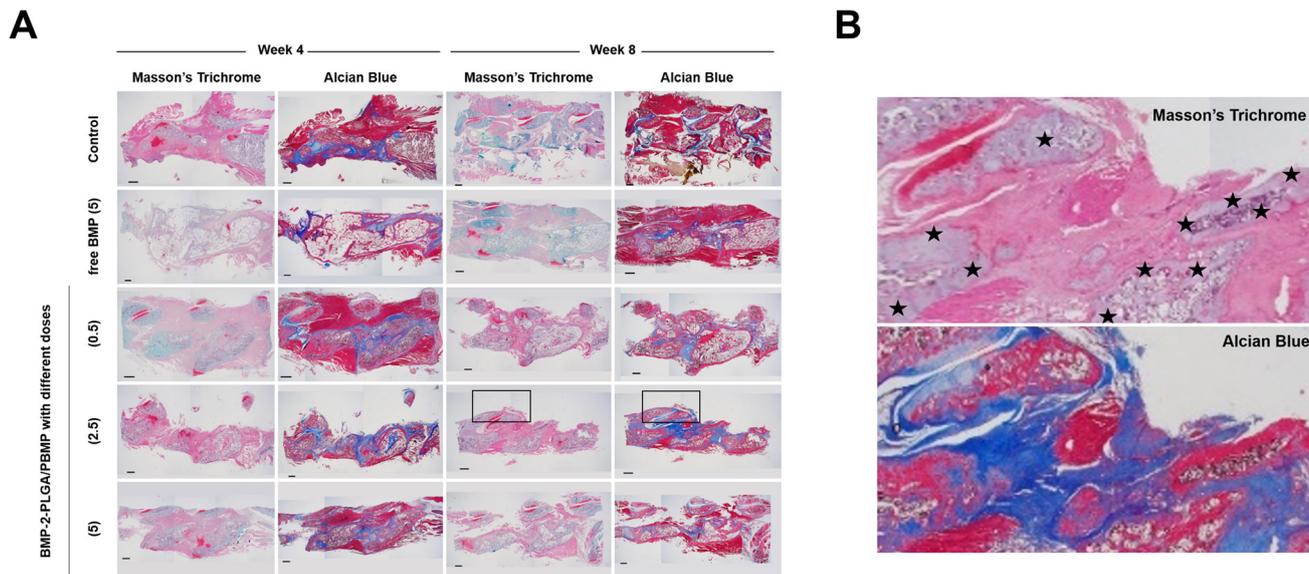
Fig. 9 Histological evaluation of surgical sections after the spine fusion surgery in the rat model. Samples were stained with Masson's trichrome (for bone matrix) and Alcian blue (for cartilage). (Scale bar = 1000 μm.) (A) Representative images of the bone formation after 4 and 8 weeks of spinal fusion surgery. (B) High magnification images of boxed regions in the BMP(2.5)-PLGA/PBMP group at 8 weeks. The star-shaped markers indicate the cortical bone of the transverse process.

stains cartilage and collagen in blue and the Masson-trichrome staining shows the newly formed bones and collagen in green.[44,45] After 4 weeks, all groups showed significantly large areas of newly formed cartilage, bones, and collagen. However, after 8 weeks, most groups showed significantly decreased blue- or green-stained areas. Only the BMP(2.5)-PLGA/PBMP group demonstrated pronounced and sustained staining of newly formed bone and cartilage through 8 weeks, with particularly strong signals at the cortical bone interface, as shown in the magnified images (Fig. 9B). These findings suggest that the sustained release of rhBMP-2 from PLGA/PBMP microparticles effectively supported the process of new bone formation. In addition, no particles were detected in the histological images, likely due to the hydrolytic degradation of PLGA *in vivo* or their removal during the tissue processing procedures, including xylene treatment.[17,46,47]

3.8 Evaluation of ectopic bone formation after posterolateral spine fusion

Despite the strong osteogenic potential of rhBMP-2, its clinical use is often limited by side effects such as uncontrolled bone formation in non-target sites. This ectopic bone formation typically results from the uncontrolled diffusion of rhBMP-2 to unintended sites.[10] Therefore, we expected that our BMP-PLGA/PBMP microparticles with strong bone binding affinity would minimize such off-target effects by localizing rhBMP-2 to the defect sites. The micro-CT images in Fig. 10A demonstrate examples of normal bone formation and ectopic bone formation in our posterolateral spinal fusion surgery model. The bone growth outside of the intended fusion site between the L4 and L5 transverse processes where rhBMP-2-

treated AIB was placed is defined as ectopic bone. These areas of ectopic bone are indicated as arrows in the micro-CT images in Fig. 10B and Fig. S5–S9.

Fig. 11 and Table 2 summarize the occurrence of ectopic bone formation at 4 weeks and 8 weeks post-surgery. At 4 weeks, the free BMP(5) group showed a significantly higher incidence of ectopic bone formation (7/9) compared to the control group (1/10). In contrast, the PLGA/PBMP microparticle groups demonstrated a profound reduction in this side effect. No ectopic bone formation was observed in the BMP(0.5)-PLGA/PBMP (0/5) and BMP(5)-PLGA/PBMP (0/5) groups, and only a single case was observed in the BMP(2.5)-PLGA/PBMP group (1/10). This trend continued at the 8 week time point, with the free BMP(5) group maintaining a high incidence (6/10), while the particle groups showed minimal to no ectopic bone formation: BMP(0.5)-PLGA/PBMP (0/5), BMP(2.5)-PLGA/PBMP (1/10), and BMP(5)-PLGA/PBMP (0/5).

While the free BMP(5) group was highly effective in promoting bone growth (126 mm^3 at 4 weeks, Fig. 8B), this came at the cost of substantial ectopic bone formation, likely due to the non-localized diffusion and uncontrolled burst release of rhBMP-2. In contrast, the BMP(2.5)-PLGA/PBMP and BMP(5)-PLGA/PBMP groups achieved remarkable bone volume increases (56 mm^3 and 63 mm^3, respectively, at 8 weeks, Fig. 8C) with negligible ectopic bone formation. This strongly suggests that the high binding affinity of PBMP for the bone surface effectively confined rhBMP-2 diffusion to the defect site.

Notably, no statistically significant difference in ectopic bone formation was observed among the three particle dosage groups. The complete absence of ectopic bone in the BMP(0.5)-PLGA/PBMP and BMP(5)-PLGA/PBMP groups, compared
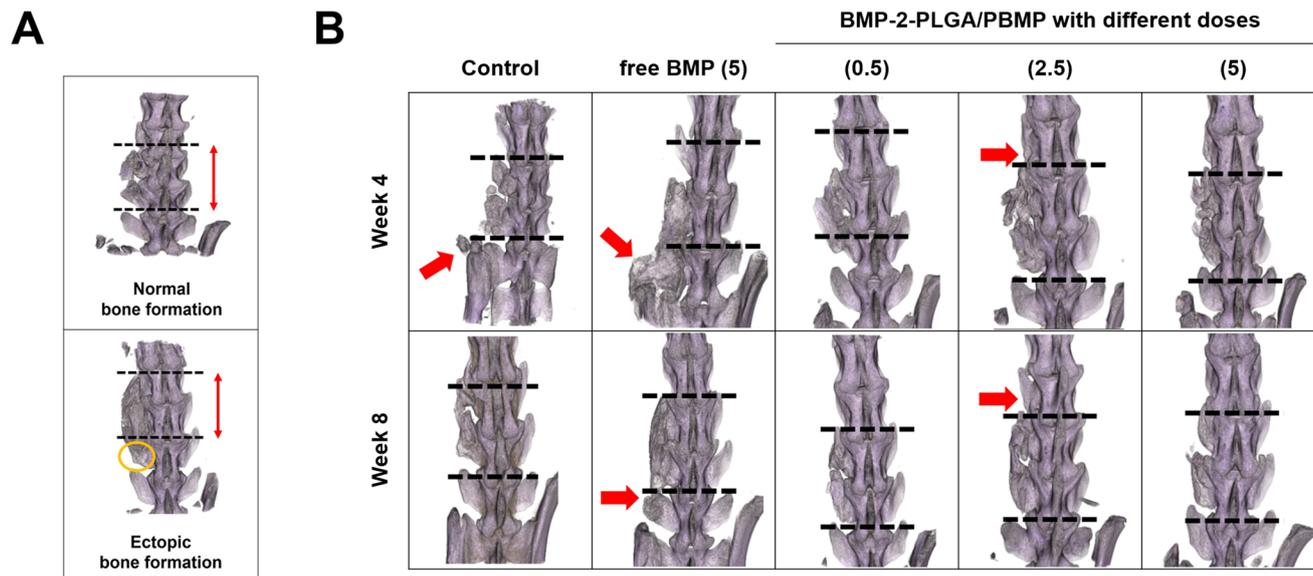
Fig. 10 Micro-CT analysis of ectopic bone formation in a rat spinal fusion model. (A) Representative micro-CT images defining the assessment of ectopic bone. The surgical site between the L4 and L5 transverse processes, where AIB was placed to induce synostosis, is marked by bilateral red arrows. Bone growth outside of the surgical region (indicated by the yellow circle) is defined as ectopic bone formation. (B) Representative micro-CT images of the surgical sites at 4 and 8 weeks post-surgery, with red arrows indicating regions of ectopic bone formation.
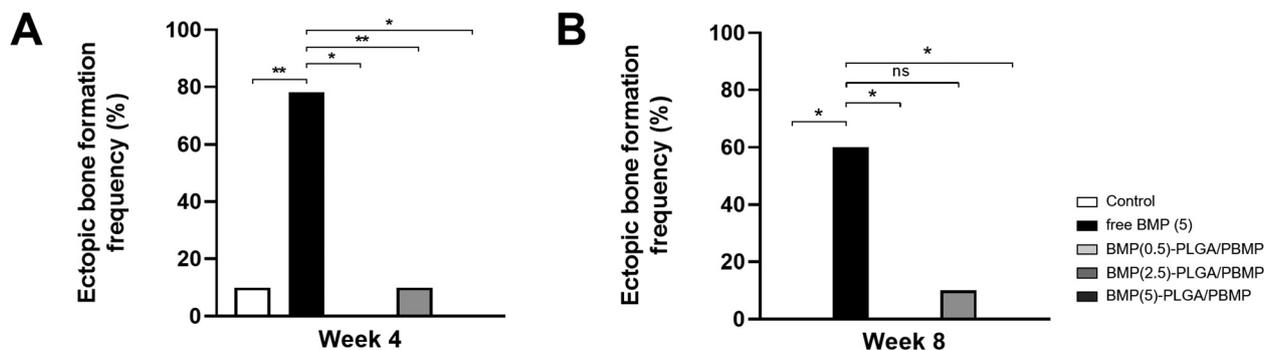

Fig. 11 Comparison of ectopic bone formation frequency after the spine fusion surgery in the rat model. Ectopic bone formation frequency at week 4 (A) and at week 8 (B). The statistical analysis was performed using Fisher's exact test. * and ** indicates $0.01 \leq p < 0.05$ and $p < 0.01$, respectively. ns means not significant.

Table 2 Comparison of ectopic bone formation after the spine fusion surgery in the rat model

	Control	free BMP (5)	BMP (0.5)-PLGA/PBMP	BMP (2.5)-PLGA/PBMP	BMP (5)-PLGA/PBMP
Week 4	1/10	7/9	0/5	1/10	0/5
Week 8	0/9	6/10	0/5	1/10	0/5

to the single case in the BMP(2.5)-PLGA/PBMP group, is likely due to the smaller animal cohort sizes ($n = 5$ for BMP(0.5)-PLGA/PBMP and BMP(5)-PLGA/PBMP *vs.* $n = 10$ for BMP(2.5)-PLGA/PBMP) rather than a dose-dependent effect. The consistent and dramatic reduction of ectopic bone formation across all PLGA/PBMP groups compared to that with free rhBMP-2 underscores the system's ability to provide safe and targeted bone regeneration.

4. Conclusion

We successfully encapsulated rhBMP-2 in PLGA microparticles coated with the calcium-binding polymer PBMP, enabling localized delivery of rhBMP-2 for enhanced bone regeneration without side effects at spine fusion surgery sites. The strong binding affinity of BMP-2-PLGA/PBMP to calcium-rich bone surfaces facilitated sustained release of the encapsulated protein

over several weeks. In a posterolateral spine fusion rat model, BMP-2-PLGA/PBMP maintained bone regeneration activity for up to 8 weeks. More importantly, a significant reduction in ectopic bone formation validated the efficacy of localized delivery of rhBMP-2, with therapeutic action confined to the target site. Despite these promising outcomes, this study was limited by small *in vivo* group sizes, which precluded quantitative histological scoring. Future investigations should incorporate larger animal cohorts to enable robust statistical analysis.

We believe that PLGA/PBMP microparticles hold substantial clinical potential for patients requiring enhanced bone healing—regardless of age or medical history—by maximizing bone growth factor efficacy while minimizing adverse effects. Unlike bulk scaffolds, our microparticles offer superior surface area-to-volume ratios that promote targeted adhesion at defect sites through bone-targeting coatings, thereby reducing ectopic mineralization risks. The simplified dip-coating method with bone-binding polymers further enables efficient multi-drug encapsulation and precise release control. However, optimization of encapsulation efficiency for hydrophilic proteins remains necessary to maximize therapeutic efficacy. Future studies could explore co-encapsulation of early osteogenesis promoters (*e.g.*, FGFs) or anti-inflammatory agents to achieve synergistic therapeutic outcomes.

Author contributions

M. Kim performed most *in vitro* experiments and wrote the primary manuscript. J. K. performed most *in vivo* experiments and wrote the primary manuscript. M. Kang designed and performed *in vitro* experiments. S. N. and C.-H. K. designed the experiments and analyzed the results. Y. L. and S. B. P. designed and supervised the whole projects as corresponding authors wrote the primary manuscript.

Conflicts of interest

The authors declare no competing interests.

Data availability

The data supporting this article have been included as part of the supplementary information (SI). Supplementary information: Table S1 and Fig. S1–S9. See DOI: https://doi.org/10.1039/d5bm01536g.

Acknowledgements

References

1 S. Bolamperti, I. Villa and A. Rubinacci, *Bone Res.*, 2022, **10**, 48.

2 A. Infante and C. I. Rodriguez, *Stem Cell Res. Ther.*, 2018, **9**, 244.

3 R. Zura, M. J. Braid-Forbes, K. Jeray, S. Mehta, T. A. Einhorn, J. T. Watson, G. J. Della Rocca, K. Forbes and R. G. Steen, *Bone*, 2017, **95**, 26–32.

4 E. G. Meinberg, D. Clark, K. R. Miclau, R. Marcucio and T. Miclau, *Injury*, 2019, **50**(Suppl 1), S62–S65.

5 B. A. Foulke, A. R. Kendal, D. W. Murray and H. Pandit, *Maturitas*, 2016, **92**, 49–55.

6 T. T. Roberts and A. J. Rosenbaum, *Organogenesis*, 2012, **8**, 114–124.

7 W. Wang and K. W. K. Yeung, *Bioact. Mater.*, 2017, **2**, 224–247.

8 A. Szwed-Georgiou, P. Płociński, B. Kupikowska-Stobba, M. M. Urbaniak, P. Rusek-Wala, K. Szustakiewicz, P. Piszko, A. Krupa, M. Biernat, M. Gazińska, M. Kasprzak, K. Nawrotek, N. P. Mira and K. Rudnicka, *ACS Biomater. Sci. Eng.*, 2023, **9**, 5222–5254.

9 A. Oryan, S. Alidadi, A. Moshiri and A. Bigham-Sadegh, *BioFactors*, 2014, **40**, 459–481.

10 A. W. James, G. LaChaud, J. Shen, G. Asatrian, V. Nguyen, X. Zhang, K. Ting and C. Soo, *Tissue Eng., Part B*, 2016, **22**, 284–297.

11 M. Lykissas and I. Gkiatas, *World J. Orthop.*, 2017, **8**, 531–535.

12 A. Arias-Betancur, N. Badilla-Wenzel, A. Astete-Sanhueza, N. Farfan-Beltran and F. J. Dias, *Jpn. Dent. Sci. Rev.*, 2022, **58**, 316–327.

13 X. Chen, B. Tan, Z. Bao, S. Wang, R. Tang, Z. Wang, G. Chen, S. Chen, W. W. Lu, D. Yang and S. Peng, *Biomaterials*, 2021, **277**, 121117.

14 B. B. Seo, H. Choi, J. T. Koh and S. C. Song, *J. Controlled Release*, 2015, **209**, 67.

15 W. Zhuang, G. Ye, J. Wu, L. Wang, G. Fang, Z. Ye, G. Lai, X. Qiu and H. Sang, *Biomater. Adv.*, 2022, **133**, 112619.

16 D. Tateiwa, S. Nakagawa, H. Tsukazaki, R. Okada, J. Kodama, J. Kushioka, Z. Bal, Y. Ukon, H. Hirai and T. Kaito, *Sci. Rep.*, 2021, **11**, 16924.

17 H. K. Makadia and S. J. Siegel, *Polymers*, 2011, **3**, 1377–1397.

18 Y. Xu, C. S. Kim, D. M. Saylor and D. Koo, *J. Biomed. Mater. Res., Part B*, 2017, **105**, 1692–1716.

19 K. Park, S. Skidmore, J. Hadar, J. Garner, H. Park, A. Otte, B. K. Soh, G. Yoon, D. Yu, Y. Yun, B. K. Lee, X. Jiang and Y. Wang, *J. Controlled Release*, 2019, **304**, 125–134.

20 R. Ma, Y. Su, R. Cao, K. Wang and P. Yang, *Int. J. Nanomed.*, 2023, **18**, 5055–5072.

21 X. Wang, W. Chen, Z. Chen, Y. Li, K. Wu and Y. Song, *Contrast Media Mol. Imaging*, 2022, **2022**, 1081957.

22 C. A. Tannoury and H. S. An, *Spine J.*, 2014, **14**, 552–559.

23 M. Kang, S. Kim, H. Kim, Y. Song, D. Jung, S. Kang, J. H. Seo, S. Nam and Y. Lee, *ACS Appl. Mater. Interfaces*, 2019, **11**, 7686–7694.

24 S. N. Hong, M. Kim, J. A. Park, M. Kang, H. Cha, S. Park, J. K. Kim, J. Pac, Y. Seo, S. Kim, M. Kim, D. W. Kim and Y. Lee, *Pharmaceutics*, 2022, **14**, 546.

25 M. E. Fox, F. C. Szoka and J. M. J. Fréchet, *Acc. Chem. Res.*, 2009, **42**, 1141–1151.

26 E. Swider, O. Koshkina, J. Tel, L. J. Cruz, I. J. M. de Vries and M. Srinivas, *Acta Biomater.*, 2018, **73**, 38–51.

27 M. Chatterjee and N. Chanda, *Mater. Adv.*, 2022, **3**, 837–858.

28 J. W. Hustedt and D. J. Blizzard, *Yale J. Biol. Med.*, 2014, **87**, 549–561.

29 S. Kang, M. Lee, M. Kang, M. Noh, J. Jeon, Y. Lee and J.-H. Seo, *Acta Biomater.*, 2016, **40**, 70–77.

30 H. Zhao, Y. Yang, X. Shu, Y. Wang, S. Wu, Q. Ran and J. Liu, *Comput. Mater. Sci.*, 2018, **152**, 43–50.

31 S.-H. Jeong, K. T. Nguyen, M. T. Nguyen, J.-S. You, B.-H. Kim, H.-C. Choe and S.-G. Ahn, *ACS Biomater. Sci. Eng.*, 2023, **9**, 1377–1390.

32 S. Nepal, J. Si, S. Ishikawa, M. Nishikawa, Y. Sakai, A. M. Akimoto, H. Okada, S. Ohba, U.-i. Chung, T. Sakai and H. Hojo, *Regener. Ther.*, 2024, **25**, 24–34.

33 Q.-l. Li, Y.-x. Wu, Y.-x. Zhang, J. Mao and Z.-x. Zhang, *RSC Adv.*, 2024, **14**, 1527–1537.

34 Z. Shi, Q. Zhong, Y. Chen, J. Gao, X. Pan, Q. Lian, R. Chen, P. Wang, J. Wang, Z. Shi and H. Cheng, *Int. J. Nanomed.*, 2021, **16**, 5603–5619.

35 M. J. Kim, J.-H. Park, J. M. Seok, J. Jung, T. S. Hwang, H.-C. Lee, J. H. Lee, S. A. Park, J.-H. Byun and S. H. Oh, *Biofabrication*, 2024, **16**, 025014.

36 M. Izumiya, M. Haniu, K. Ueda, H. Ishida, C. Ma, H. Ideta, A. Sobajima, K. Ueshiba, T. Uemura, N. Saito and H. Haniu, *Int. J. Mol. Sci.*, 2021, **22**, 7752.

37 X. W. Liu, B. Ma, Y. Zi, L. B. Xiang and T. Y. Han, *Eur. J. Histochem.*, 2021, **65**, 3195.

38 S. B. Park, S. H. Park, N.-H. Kim and C. K. Chung, *Spine J.*, 2013, **13**, 1273–1280.

39 S. B. Park, H.-J. Yang, C. H. Kim and C. K. Chung, *J. Korean Neurosurg. Soc.*, 2017, **60**, 348–354.

40 T. Hu, S. A. Abbah, S. Y. Toh, M. Wang, R. W. M. Lam, M. Naidu, G. Bhakta, S. M. Cool, K. Bhakoo, J. Li, J. C.-H. Goh and H.-K. Wong, *J. Spine*, 2015, **15**, 2552–2563.

41 M. Refaat, E. O. Klineberg, M. C. Fong, T. C. Garcia, J. K. Leach and D. R. Haudenschild, *Spine*, 2016, **41**, E829–e836.

42 S. N. Parikh, *Orthopedics*, 2002, **25**, 1301–1309.

43 H.-S. Sohn and J.-K. Oh, *Biomater. Res.*, 2019, **23**, 9.

44 D. Rigueur and K. M. Lyons, *Methods Mol. Biol.*, 2014, **1130**, 113–121.

45 A. K. Leonard, E. A. Loughran, Y. Klymenko, Y. Liu, O. Kim, M. Asem, K. McAbee, M. J. Ravosa and M. S. Stack, in *Methods in Cell Biology*, ed. R. P. Mecham, Academic Press, 2018, vol. 143, pp. 79–95.

46 E. M. Elmowafy, M. Tiboni and M. E. Soliman, *J. Pharm. Invest.*, 2019, **49**, 347–380.

47 L. Lu, S. J. Peter, M. D. Lyman, H.-L. Lai, S. M. Leite, J. A. Tamada, S. Uyama, J. P. Vacanti, L. Robert and A. G. Mikos, *Biomaterials*, 2000, **21**, 1837–1845.